Non-local diffusion-based biomarkers in patients with cocaine use disorder

Alfonso Estudillo-Romero, Raffaella Migliaccio, Bénédicte Batrancourt, Pierre Jannin, John S H Baxter

Neuroimage: Reports 4 (2024) 100202

Contents lists available at ScienceDirect

Neuroimage: Reports

journal homepage: www.sciencedirect.com/journal/neuroimage-reports

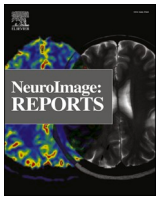

Non-local diffusion-based biomarkers in patients with cocaine use disorder

Alfonso Estudillo-Romero [a], Raffaella Migliaccio [b], Bénédicte Batrancourt [b], Pierre Jannin [a], John S.H. Baxter [a,*]

[a] Laboratoire de Traitement du Signal et de l'Image (LTSI- INSERM UMR 1099), Université de Rennes, Rennes, 35000, France
[b] Institut du Cerveau, Paris, France

ARTICLE INFO

Keywords:
Cocaine use disorder
Diffusion tensor imaging
Voxel-based diktiometry
Sparse principal components analysis

ABSTRACT

Cocaine use disorder (CUD) is widely known to result in neurological reconfiguration which can be observed via local diffusivity characteristics of the brain. These changes can be highly correlated while simultaneously variable across patients with different comorbidities or histories of substance use. This implies that more complex neuroimage analysis tools may be necessary to better detect specific biomarkers that vary across these dimensions. We investigated white and gray matter integrity using voxel-based diktiometry (VBD) on whole brain diffusion tensor images (DTI) across a database of CUD patients and healthy controls using a purely data-driven approach. These VBD maps reveal significant cortical and subcortical differences that are indicative of these neural modifications including the insula, cerebellum, ventricles, thalamo-cortical radiations, and corpus callosum bundles. In order to disambiguate these results and investigate the heterogeneity of CUD, the VBD maps have been decomposed into five decorrelated biomarkers: one in the region surrounding the left insula, one implicating the corpus callosum, two concentrated in the left cerebellum, and the last concerning a proximal region of the interhemispheric fissure which serve as potential biomarkers playing a role in CUD. These decorrelated biomarkers have themselves been correlated with consumption patterns and psychiatric and borderline personality disorder scores on the CUD patient group. This preliminary approach to using machine learning techniques to both detect and disambiguate complex non-linear patterns shows promise for better understanding complex and heterogeneous disorders such as CUD.

1. Introduction

Cocaine is one of the most highly used illicit substances in the world with approximately 0.35% of the adult population experiencing some form of cocaine use disorder (CUD) (Peacock et al., 2018) with much higher rates being seen in specific countries such as 1.7% in the United States in 2021 (National Survey on Drug Use and Health, 2021).

Neurological, emotional, and cognitive changes have been observed in patients with CUD resulting in an increase in impulsivity and reward-seeking behaviours (Spronk et al., 2013; Jiménez et al., 2019; Wei et al., 2021; Suchting et al., 2021; Ceceli et al., 2022). In general, drug abuse can be conceptualized as a cycle consisting of three stages: binge/intoxication, withdrawal/negative affect and preoccupation/anticipation or craving (Koob and Volkow, 2010). The brain networks that have been identified in this cycle include the ventral tegmental area (VTA) and ventral striatum at the binge/intoxication stage, the extended amygdala during the withdrawal/negative affect stage and, a more distributed network that includes the orbitofrontal cortex, dorsal striatum, prefrontal cortex, basolateral amygdala, hippocampus, and insula at the preoccupation/anticipation stage and the cingulate gyrus, dorsolateral prefrontal, and inferior frontal cortices in disrupted inhibitory control and impulsivity that is hypothesized to contribute to relapse (Koob and Volkow, 2010; Lesage and Stein, 2016).

Diffusion imaging, specifically Diffusion Tensor Imaging (DTI), offers an interesting research tool for better understanding addiction disorders such as CUD. This imaging modality allows for the measurement of structural diffusivity changes in the white matter (WM) and cerebrospinal fluid (CSF) systems that can elicit information regarding tissue composition and even micro-structural information. The volume and microstructural integrity of these systems can be sensitively measured via DTI and have been the subject of several studies comparing healthy controls with patients suffering from CUD. The extent of these alterations may be related to the duration and severity of CUD and might even be used to recommend treatments or to monitor their efficacy.

* Corresponding author.
E-mail address: john.baxter@univ-rennes.fr (J.S.H. Baxter).

https://doi.org/10.1016/j.ynirp.2024.100202
Received 13 February 2024; Received in revised form 25 March 2024; Accepted 26 March 2024
Available online 26 April 2024

Using DTI for investigating neurological disorders however often required a computational framework, such as tractography and fibre clustering, to simplify it and to investigate particular phenomenon. Although tractography itself is not standardized and thus poses problems for standardized clinical applications (Pujol et al., 2015), it has lead to many interesting findings, summarised in the following subsection, but leaves space for less-constrained approaches.

1.1. Neurological diffusivity changes in CUD

A meta-analysis using tract-based spatial statistics (TBSS) including articles from 2006 to 2020 has showed consistent WM integrity decline among eight selected studies on individuals with CUD compared to healthy controls (HC) using DTI images of the whole brain (Suchting et al., 2021). More specifically, the consistent pathology observed across the studies involves the genu of the corpus callosum (gCC) which may be implicated on some longer term cognitive effects as impairment to response inhibition, recall, cognitive flexibility, behaviour adaptation, reward processing, and psychomotor performance.

In another study using TBSS (Tondo et al., 2021), showed that global fractional anisotropy (FA) significant decreases and mean diffusivity (MD) increases in the CUD group with respect to the HC group along the major WM tracts. Within the CUD group, the FA was found to be negatively associated with the number of years of cocaine consumption and with 12 FA clusters identified including the cingulum bundle, corpus callosum, uncinate fasciculus, the gCC and the body of the corpus callosum (bCC).

Previous work by Rasgado-Toledo et al. (2022) using a technique based on neurite orientation dispersion and density imaging (NODDI) analysis explored microstructural WM and gray matter (GM) differences between HC and CUD patients along the longitudinal fasciculus, cingulum, hippocampus, forceps minor, and uncinate fasciculus, as well as in the frontal and parieto-temporal lobes. Moreover, they have also detailed correlations with impulsivity, onset age of cocaine use, and weekly dosage.

A more recent study has investigated generalized and acute and/-or specific drug effects on the WM and found decreased anisotropy and increased diffusivity on CUD associated with longer periods of regular use. However, association with craving suggested greater impairments with more recent use (Gaudreault et al., 2023).

In terms of cortical targets for treating addiction, the anterior cingulate cortex (ACC), the inferior frontal gyrus, supramarginal gyrus, middle temporal gyrus, and precuneus have commonly been used for that purpose (Hammond et al., 2019; Zhao et al., 2021).

Changes in consumption patterns have been positively associated with impulsiveness (Hulka et al., 2015) where patients that increased their consumption after one year follow up exhibited higher scores with respect to those who decreased it.

Reduced connectivity between the bilateral putamen, posterior insula, and right post-central gyrus circuit has been observed in CUD patients and has also been associated with higher motor impulsivity with respect to HC (McHugh et al., 2013).

1.2. Contributions

To the best of our knowledge, all previous diffusivity-based findings of the brain regions being altered not only due to cocaine abuse but also for general substance abuse disorders (SUD) have used methods relying on TBSS and subsequent traditional statistical or machine learning analysis at a very local level. That is, they comprise of predictors from diffusivity characteristics of individual tracts. This local approach allows for specific regions to be analysed although the particular analyses used cannot observe non-linear and often diffuse patterns occurring throughout the entire brain.

In this work, we analysed for the first time the whole brain diffusivity characteristics of CUD patients in a non-local manner by means of voxel-based diktiometry (VBD) (Estudillo-Romero et al., 2022) which uses a sequence of CNNs that classifies CUD patients from HC. This approach is fully inductive and data-driven, providing a global view of neurological changes in CUD that affect diffusion in the brain which we then compare to traditional voxel-based analysis (VBA). To analyse the heterogeneity of CUD patients (both in terms of imaging and clinical variables), sparse principal component analysis (sPCA) is performed on the VBD results, developing individualised biomarkers that can be correlated with clinical characteristics of CUD individuals. In Section 2 we present the demographic, clinical and imaging information of the used dataset as well as the technical methods employed for the analysis. The results of said analysis will be presented in Section 3 in the form of sensitivity maps, specific biomarker components, and their correlation with clinical/behavioural scores. Our interpretation of these results in light of recent literature as well as the limitations of our current work are presented in Section 4. Given the purely inductive nature of the research, the exact results are preliminary but nevertheless show the potential for machine learning to discover and disambiguate complex non-local biomarkers that would otherwise be invisible to existing population neuroimaging methods.

2. Methods

2.1. Voxel-based diktiometry

Voxel-Based Diktiometry (VBD) is a purely data-driven methodology that has been recently proposed (Estudillo-Romero et al., 2022) to investigate biomarkers by means of a combination of an ensemble of simple convolutional neural networks (CNNs) and the analysis of their sensitivity maps into a standard common space. Such sensitivity maps are calculated with respect to some well-known diffusivity measures such as the mean diffusivity, the anisotropy, and the fractional anisotropy. The sensitivity maps are calculated from the testing images set after the CNN has been trained. The analysis follows a population based VBA of the sensitivity map with respect to each diffusivity measure in a common space. The diktiometry maps are then obtained from the statistical analysis of the voxel population passing a significance threshold within a minimum cluster size. The benefit of VBD compared to other methods is that it retains the whole-brain focus of traditional VBA while also allowing for complex non-local effects to be observed. These effects are determined entirely unguidedly by the computer and thus represent the most salient alterations caused by CUD.

One specific aspect of VBD is the transformation of the sensitivity information into metrics that are more easily understood. In the case of DTI, the underlying machine learning algorithm is applied directly to the elements of the diffusion tensor, which are not particularly human-understandable and is heavily sensitive to the exact orientation of objects in the image. Often, this tensor is understood instead through orientation-insensitive metrics, notable mean diffusivity (MD) and fractional anisotropy (FA). However, these two metrics are known to be mathematically coupled, leading to the development of anisotropy (A) and pseudo-planarity (PsPl) as metrics that are mathematically orthogonal with each other and with MD, and the former being the numerator component of FA (Estudillo-Romero et al., 2022). This orthogonality renders themselves more sensitive as a whole as they capture all of the networks' sensitivity to all orientation-insensitive features.

2.2. Patient images

The participants in this study included 69 CUD patients and 58 HC from the SUDMEX CONN dataset (Angeles-Valdez et al., 2022). All the data in this public dataset was collected after written and verbal informed consent of the patients and the data collection was approved by the Ethics Committee of the Instituto Nacional de Psiquiatria "Ramón de la Fuente Muñiz" (Angeles-Valdez et al., 2022). We excluded patients with missing T1 or diffusion-weighted MRI images.

The anatomical T1 image was acquired using a 3D Fast Field Echo (FFE) sequence with 1 mm isotropic resolution, TR/TE = 7/3.5 ms, field of view = 240 mm^2, matrix 240 × 240 mm, resulting in 160 slices along the sagittal plane. The diffusion DWI-HARDI sequences were acquired using a single spin echo (TR/TE = 8600/126.78 ms), with 2 mm isotropic resolution, field of view 224 mm^2, matrix 112 × 112 mm, phase encoding direction from posterior to anterior, resulting in 50 slices along the axial plane. The DWI-HARDI sequence included a total of 136 gradient directions (8 directions for the b0, 36 for the b-value 1000 s/mm^2 and 92 for the b-value 3000 s/mm^2) (Angeles-Valdez et al., 2022).

2.3. Clinical measurements

A summary of the demographic and clinical data is provided in Table 1 for all participants including cocaine, tobacco, and alcohol consumption patterns as well as: attentional impulsiveness measured by attention and cognitive instabilities; motor impulsiveness and non planning impulsiveness evaluated by the Barratt Impulsiveness Scale (BIS-11); and the clinical global impression scale for borderline personality disorder (CGI-BPD). We also calculated composite values of the medical, employment, alcohol use, drug use, legal, family, and psychiatric statuses evaluated by the Addiction Severity Index (ASI) following Mclellan et al. (1992). Additionally, we included in this study the evaluation of the Symptom Checklist-90-Revised (SCL-90-R), the Structured Clinical Interview for DSM-IV axis II personality disorders (SCID-II) and the World Health Organization Disability Assessment Schedule 2.0 (WHODAS 2.0) already contained in the dataset. Statistical tests were performed on each of the clinical measurements comparing the CUD patient group with the HC group using Student's *t*-tests on continuous variables and χ^2-tests on categorical variables. Statistical testing did not find a significant difference between both groups in terms of gender or age, but did find differences in terms of smoking behaviour and impulsiveness.

2.4. Preprocessing

First, we used standard preprocessing tools for noise removal on both T1 and DWI sequences. We then corrected eddy currents and subject motion using FSL (Andersson and Sotiropoulos, 2016) on the DWI sequences. Finally, we calculated the DTI by means of weighted least squares (WLS) fitting method included in SlicerDMRI (Norton et al., 2017).

The size of the DTI images was standardised to 104 × 104 × 50 (in the sagittal, coronal and axial planes, respectively) by adding or removing background slices as needed at each extreme in the sagittal and coronal portions of the volume.

2.5. CNN training

We trained a simple CNN architecture in PyTorch shown in Fig. 1. Given the small amount of data, we tested the CNN's learning effectiveness by measuring the classification accuracy in a 10-fold cross-validation manner. We trained the CNN for 230 epochs using a batch size of 11 DTI samples. The training was started with a learning rate (l_r) of 1.2 × 10^{-5} and gradually decreased by 5% every 30 epochs. We optimised the CNN using Adam optimiser with L2 regularisation set to 0.0025 and added 2% dropout layers as shown in Fig. 1.

We measured the binary cross-entropy with logit loss (BCEWithLogitsLoss) and the balanced accuracy on both the training and testing subsets for each fold every epoch:

$$\text{Balanced accuracy} = \frac{1}{2}\left(\frac{TP}{P} + \frac{TN}{N}\right) \quad (1)$$

The CNN, $N(\cdot)$, receives a DTI image of a subject p as input and produces

Table 1
Participant demographic and clinical data comparing cocaine use disorder (CUD) patients and healthy controls (HC).

		CUD patients ($n = 69$)	HC ($n = 58$)	Statistics	
Women		($n = 8$)	($n = 11$)	$\chi^2 = 0.83$	$p = 0.363$
Age		31.22 (7.29)	30.66 (8.36)	$t = -0.405$	$p = 0.686$
Cocaine consumption					
Age onset		($n = 66$) 20.95 (5.73)	n/a		
Years consuming		($n = 66$) 10.14 (6.86)	n/a		
Average weekly dose		($n = 65$)	n/a		
0 − 0.33 g		7			
0.33 − 0.66 g		16			
0.66 − 4 g		29			
4 − 8 g		7			
8 − 10 g		3			
> 10 g		3			
Cocaine craving now		($n = 67$) 142.58 (44.63)	n/a		
Years of tobacco use		($n = 58$) 13.71 (8.15)	($n = 50$) 6.22 (7.83)	$t = -4.847$	$p = 4e^{-6}$
Years of alcohol use		($n = 64$) 13.64 (8.72)	n/a		
BIS		($n = 59$)	($n = 48$)		
	Attention	17.24 (5.19)	13.12 (4.57)	$t = -4.296$	$p = 4e^{-5}$
	Motor	19.15 (7.59)	14.17 (6.46)	$t = -3.611$	$p = 5e^{-4}$
	Non planned	25.02 (7.49)	17.69 (7.07)	$t = -5.161$	$p = 1e^{-6}$
BIS total		61.41 (14.84)	44.98 (14.91)	$t = -5.682$	$p < 1e^{-6}$
ASI composite (0–1)		($n = 59$)	n/a		
Medical		0.16 (0.26)			
Alcohol use		0.21 (0.22)			
Psychiatric		0.34 (0.27)			
CGI-BPD		($n = 53$) 3.10 (1.18)	($n = 32$) 1.39 (0.64)	$t = -7.528$	$p < 1e^{-6}$
SCID-II		($n = 60$)	($n = 43$)		
A	Paranoid	3.17 (2.85)	1.93 (2.49)	$t = -2.288$	$p = 0.0242$
	Schizoid	2.45 (2.30)	1.79 (1.60)	$t = -1.622$	$p = 0.108$
	Schizotypal	1.62 (1.97)	1.19 (1.95)	$t = -1.099$	$p = 0.275$
B	Antisocial	2.63 (3.77)	0.91 (1.44)	$t = -2.854$	$p = 0.005$
	Borderline	6.07 (4.99)	1.74 (2.42)	$t = -5.245$	$p < 1e^{-6}$
	Histrionic	2.45 (2.70)	2.07 (1.79)	$t = -0.804$	$p = 0.423$
	Narcissist	3.23 (3.14)	2.44 (2.15)	$t = -1.428$	$p = 0.156$
C	Avoidant	1.90 (2.01)	1.30 (1.61)	$t = -1.615$	$p = 0.109$
	Dependent	2.30 (2.27)	0.74 (1.03)	$t = -4.190$	$p < 6e^{-5}$
	Obsessive-compulsive	2.78 (2.31)	2.84 (2.24)	$t = 0.118$	$p = 0.906$
	Passive-aggressive	2.85 (2.49)	1.09 (1.29)	$t = -4.236$	$p < 5e^{-5}$
SCL-90-R		($n = 57$)	($n = 40$)		
Anxiety		1.21 (0.95)	0.44 (0.52))	$t = -4.635$	$p = 1.1e^{-5}$
Depression		1.12 (0.93)	0.44 (0.54)	$t = -4.159$	$p < 8e^{-5}$
Hostility		0.80 (0.77)	0.42 (0.52)	$t = -2.747$	$p = 0.0072$
Interpersonal sensitivity		0.97 (0.92)	0.52 (0.69)	$t = -2.616$	$p = 0.0103$

(continued on next page)

Table 1 (*continued*)

	CUD patients ($n = 69$)	HC ($n = 58$)	Statistics	
Obsessive-compulsive	1.27 (0.97)	0.59 (0.51)	$t =$ −4.073	$p < 1e^{-4}$
Paranoid ideation	0.95 (0.96)	0.49 (0.74)	$t =$ −2.568	$p =$ 0.0118
Phobic anxiety	0.49 (0.74)	0.10 (0.23)	$t =$ −3.177	$p =$ 0.002
Psychoticism	0.81 (0.82)	0.31 (0.50)	$t =$ −3.454	$p =$ 0.0008
Global severity	1.01 (0.81)	0.42 (0.47)	$t =$ −4.142	$p < 8e^{-5}$
Positive symptom total	27.89 (22.43)	10.65 (14.04)	$t =$ −4.304	$p < 5e^{-5}$
WHODAS Total	($n = 60$) 0.16 (0.17)	($n = 43$) 0.04 (0.05)	$t =$ −4.555	$p <$ $1.5e^{-5}$

(n = count), mean (standard deviation), χ^2 = chi-squared, t = t-value, n/a = not applicable. Abbreviations: BIS, Barratt Impulsiveness Scale; ASI, Addiction Severity Index; SCID-II, Structured Clinical Interview for DSM-IV axis II personality disorders; WHODAS, World Health Organization Disability Assessment Schedule; SCL-90-R Symptom Checklist-90-Revised. A, B, C, SCID-II clusters A, B, C, respectively.

a binary output value to classify it into either being HC or CUD. By applying a sigmoid function S to the CNN's output (just before entering to the BCEWithLogitsLoss), we also calculated the probability that the given image belongs to a CUD subject as

$$P(p \text{ is CUD}) = s(N(p)) = \frac{e^{N(p)}}{1 + e^{N(p)}} \tag{2}$$

During training, we also applied data augmentation using random in-plane rotations up to ±5° and random in-plane translations up to ±5 voxels.

Whether or not the networks contain information about CUD patients is determined via a χ^2-test. Specifically, if the p-value is less than 5×10^{-4}, then we considered the network to be valid for further exploration.

2.6. Population-wise registration

Following a standard registration pipeline, we computed the linear transformation of each individual b0 first to its structural T1 image using the tool epi_reg from FSL. Using ANTs (Avants et al., 2011), we then calculated the transformation from the T1 to the MNI space by three successive intermediate rigid, affine and deformable SyN transformations (Avants et al., 2008). The above transformations were used to express the patient-specific CNN sensitivity maps (described in the next section) in the MNI common space.

2.7. Sensitivity of the CNN

We calculated for each subject i the sensitivity of the CNN $\delta N/\delta D_i$ relative to its corresponding diffusion tensor image D_i at the input of the CNN when performing classification during testing. In order to interpret the CNN's sensitivity in terms of common tensor diffusivity properties, we calculated the sensitivity of the CNN with respect to the mean diffusivity (MD, μ), the anisotropy (A, σ), the fractional anisotropy (FA), and the pseudo-planarity (PsPl, θ) (Estudillo-Romero et al., 2022):

$$\begin{aligned} \mu &= \frac{1}{3}\sum_i \lambda_i \\ \sigma &= \sqrt{\sum_i (\lambda_i - \mu)^2} \\ FA &= \sqrt{\frac{3}{2}}\sqrt{\frac{\sum_i (\lambda_i - \mu)^2}{\sum_i \lambda_i^2}} = \frac{\sqrt{3/2}\sigma}{\sqrt{3\mu^2 + \sigma^2}} \\ \theta &= arctan\left(\lambda_1 - \mu, \sqrt{1/3}\,(\lambda_2 - \lambda_3)\right) \end{aligned} \tag{3}$$

where λ_i are the eigenvalues of the diffusion tensor. While MD and FA are commonly understood metrics for tensor shape, the combination of MD, A, and PsPl are more complete as they are mathematically orthogonal and therefore uncoupled (Estudillo-Romero et al., 2022).

2.8. Voxel-based analysis statistical tests and filtering

After the sensitivities with respect to each diffusivity measure were registered into the MNI space, we calculated a t-test between the CUD and HC subjects using Statistical Parametric Mapping (SPM) in Matlab. A significance threshold of $p < 0.05$ FWE was applied to obtain positive and negative correlated diktiometry maps within a minimum cluster size of 128 mm^3. This analysis shows the regions that are most robustly relevant to distinguishing between CUD patients and HC as well as the sign of the correlation between the identified features and CUD. An equivalent traditional VBA analysis was performed directly on the registered MD, FA, A, and PsPl maps for comparison.

2.9. Sparse principal components analysis (sPCA)

One of the limitations associated with VBD is that the visualised sensitivity maps may contain multiple distinct biomarkers. This is

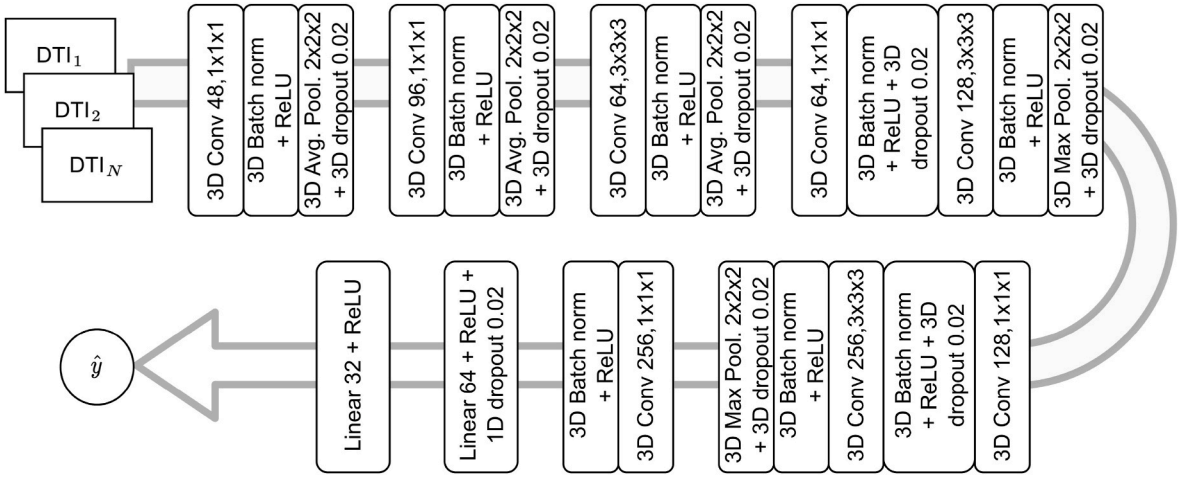

Fig. 1. Convolutional neural network architecture.

because from this singular view it is impossible to separate regions of the image that are correlated with each other from those that are not (Estudillo-Romero et al., 2022). This is problematic as different WM integrity patterns may be more easily individually explainable and may even correlate with different aspects of CUD.

In order to address this issue, we decomposed the sensitivity maps of the CUD cohort by means of sPCA (Zou et al., 2006). The aim of sPCA is to represent a set of features in a lower-dimensional space by computing its n principal components through a sparse dictionary that penalizes the eigenvalues of the traditional PCA that contain low variances. This decouples a signal into n components which are not necessarily orthogonal but that form clusters that tend to co-occur (Mairal et al., 2009). We interpret the co-occurrence as indicative of being a singular biomarker expressed in some patients more than in others. With respect to population neuro-imaging, this often implies a degree of spatial clustering although that is not guaranteed and small isolated clusters may be formed as well. Thus, we only retained spatial clusters with a minimum size using connected component analysis for spurious cluster removal.

sPCA was performed on the CUD patient cohort only as including HC would encourage the analysis to find patterns between different HC images as well which would not assist in understanding CUD. Since FA depends on MD and A (Estudillo-Romero et al., 2022), we removed redundancy and reduced computational costs by calculating the sparse components on the concatenated MD, A, and PsPl sensitivity maps. We set the parameter controlling the sparsity, α, equal to 3.5 and calculated $n = 5$ components. Then we calculated the partial Person's correlation coefficient between each component and the clinical variables from the clinical measurements presented in Section 2.3 using age and sex as covariates. Finally, we set a minimum cluster size of 128 mm^3 to remove spurious noise from the sPCA results.

3. Results

3.1. Classification accuracy

Table 2 shows the confusion matrix as well as the classification metrics computed from the 10-fold CV testing subsets. In overall, the CNN reached a balanced accuracy of 67.81% for the classification task which is significantly better than chance as supported by the chi square test (χ^2) and sufficiently accurate for use in biomarker discovery.

3.2. Voxel-based diktiometry results

Figs. 2–5 show the VBD-based maps calculated from the sensitivity of the CNN relative to MD, FA, A and PsPl respectively. These maps allow more interpretable forms of understanding the networks' sensitivity to different elements of the diffusion tensor (Estudillo-Romero et al., 2022). Traditional VBA of these characteristics did not yield any non-insignificant regions illustrating the sensitivity of non-local, non-linear biomarkers detected by VBD compared to the local and linear ones detected in traditional VBA. In the following subsections we present the cortical and subcortical regions which are positively and/or negatively associated with CUD for each diffusivity measure.

Table 2
CUD confusion matrix and classification metrics from the testing subsets using 10-fold cross validation.

		Ground truth	
		HC	CUD
Prediction	HC	40	23
	CUD	18	46
Sensitivity:		66.66 %	
Specificity:		68.96 %	
Balanced accuracy:		67.81 %	
χ^2**-statistic:**		14.611	
p**-value:**		1.32×10^{-4}	

The interpretation of features in this approach is very important as each feature could arise through different mechanisms. This is because a CNN processes the entirety of the image without consciously decomposing it into particular DTI features in particular regions. All it knows is the raw diffusion tensor at a particular voxel. This is important as, for example, CNNs can detect morphological changes but cannot express them explicitly as being morphological. Consider the network having a positive sensitivity to MD in a particular region. This could be caused in two ways: there is a structure (of relatively constant size) at that region which has a higher MD in CUD patients compared to controls; or there is a structure (of relatively constant but high diffusivity) which has a larger size in CUD patients compared to controls. Both would appear to the network as a general increase in MD in a particular region although through very different mechanisms. In addition, because these features are non-local, their sensitivities may be affected by other features. For example, the CNN may look at the asymmetry between two regions but the only way to express that is to give one a positive sensitivity and the other a negative sensitivity even if one of the sides alone could not distinguish between CUD patients and HC. This is important to take into account when considering the sensitivity features in the upcoming subsections and their interpretations in Section 4.

Due to the relatively small sample size and the relative lack of sensitivity of traditional VBA compared to VBD (Estudillo-Romero et al., 2022), the traditional VBA methods did not yield any significant clusters given this data.

3.2.1. Mean diffusivity

Regarding the CNNs' sensitivity with respect to MD, VBD showed significant positive correlated clusters with CUD from the left anterior cingulate cortex (ACC-L) to the medial superior frontal cortex (mSFC-L) on the left, as shown in Fig. 2. A small portion of the right posterior cingulate cortex (PCC-R) was also highlighted by VBD. Also, the left lateral gyrus rectus, left olfactory sulcus in the medial orbital gyrus in the frontal lobe were highlighted as positive correlated with CUD. Some positive correlated clusters were also formed in the medial temporal lobe reaching portions of the amygdala and the parahippocampal gyrus on both hemispheres. The lateral ventricles, mainly on the left hemisphere, were also highlighted including part of the gCC and the left caudate. A cluster was also located around the left posterior temporal lobe including the fusiform gryus and parts of the lingual gyrus.

The CNNs' sensitivity to MD were negatively associated with CUD as shown by the clusters found by VBD starting in both superior motor areas left and right (SMA-L, SMA-R) passing through both mSFC-L and right (mSFC-R) to finally reach up part of both the superior frontal cortices left (SFC-L) and right (SFC-R). Some clusters also formed around the insula on the right hemisphere including portions of the opercular, triangular, and orbital part of the inferior frontal gyrus. A small portion of the pre- and post-central gyrus as well as the splenium of the corpus callosum (sCC) were also highlighted. Finally, small portions of the precuneus and cuneus in both hemispheres were negatively associated with CUD.

3.2.2. Fractional anisotropy

The analysis of the CNNs' sensitivity relative to FA showed significant clusters positively correlated with CUD in the SMA-L and SMA-R passing through both mSFC-L and mSFC-R as shown in Fig. 3. The right lateral ventricle, mainly its posterior superior portions, was positively associated with CUD. Another cluster reveled portions of the vermis and lingula in the cerebellum to be positively correlated with CUD.

The CNNs' sensitivity relative to FA was negatively associated with CUD in the sulci and external cerebro-spinal fluid around the insula on the left hemisphere including portions of the opercular, triangular and orbital parts of the inferior frontal gyrus. The anterior portion of the lateral ventricle was also negatively associated with CUD.

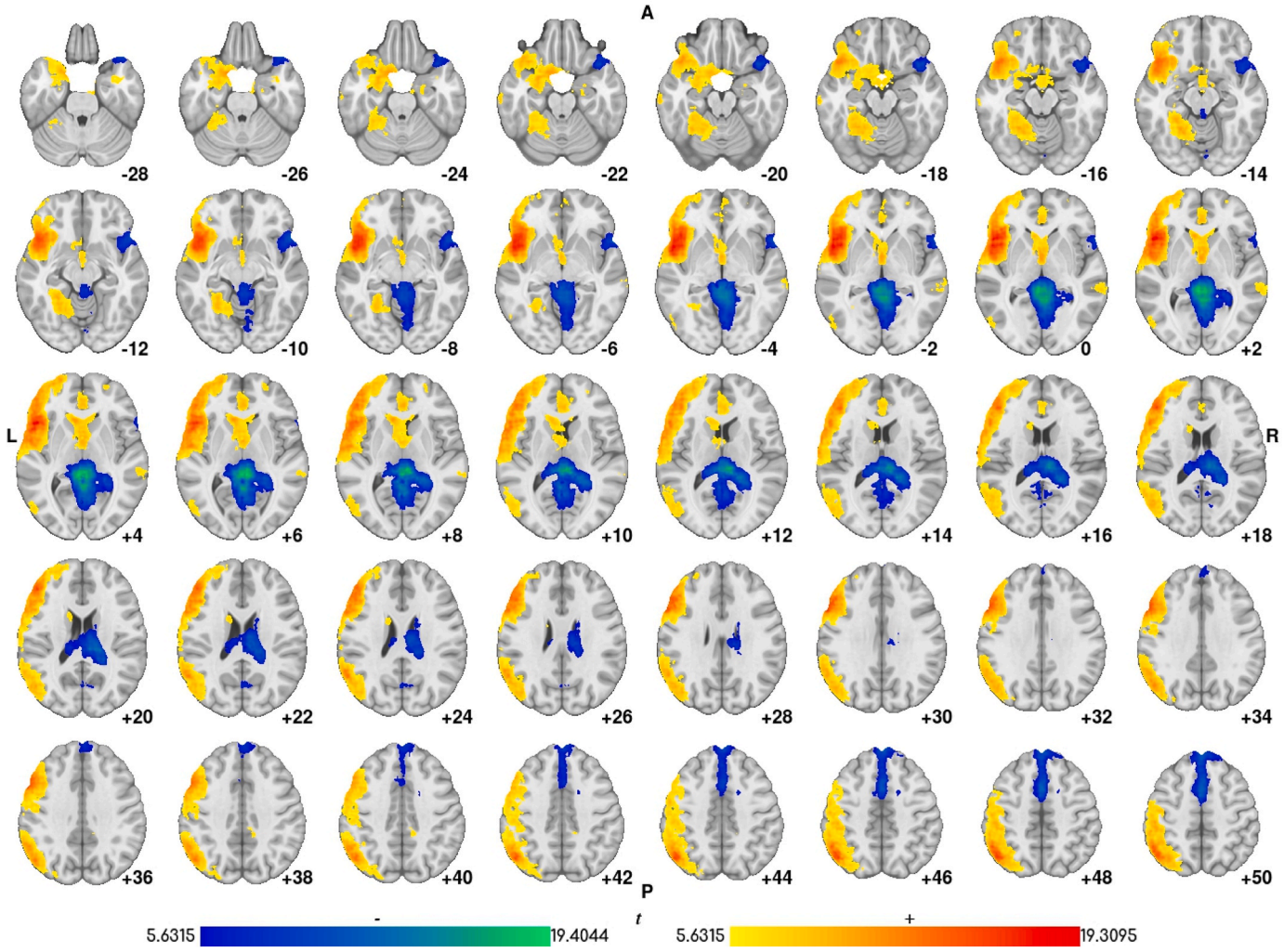

Fig. 2. Voxel-based diktiometry sensitivity results from $z = -28$ to $z = +50$ in MNI space for the mean diffusivity (MD). (Note that patient-right is shown on image-right, i.e. neurological convention.).

3.2.3. Anisotropy

A portion of the gCC as well as in the triangularis and opercular parts of the inferior frontal gyrus on the left hemisphere were found positively correlated with CUD as shown in Fig. 4. On the other side, the sCC and bCC were found to be negatively correlated with CUD. This cluster widespread through parts of both of the PCC-L and PCC-R, right hippocampus reaching up the posterior thalamic radiation and finally the posterior corona radiata on the right hemisphere. VBD also found significant clusters especially in the right hemisphere connecting the ventrolateral thalamic nucleus right (VLThal-R) and the posterior-anterior limb of the internal capsule (PLIC, ALIC) spanning through the anterior and part of the superior corona radiata on the right. The CNN sensitivity of a portion of the left thalamus was also found to be negatively associated with CUD.

3.2.4. Pseudo-planarity

We found significant clusters negatively associated with CUD regarding CNN sensitivity relative to PsPl as shown in Fig. 5. These clusters were located on the right thalamus comprising the medial pulvinar (PuM), lateral posterior (LP) and medial dorsal nucleus (MDm). Another cluster was localized around the splenium of the corpus callosum (sCC).

3.3. sPCA results

We calculated five individualised biomarkers by decomposing the CNN's sensitivities across the CUD cohort using sparse principal components analysis (sPCA). Fig. 6 shows the five principal components from a whole-brain analysis of the sensitivities relative to the MD, A, and PsPl limited to clusters of size at least 128 mm^3. Table 3 shows the partial correlations of each eigenvector of the decomposition with the clinical scores that were significant ($p < 0.05$) after removing the effects of age and sex as covariates.

3.3.1. PC1

The first decomposition or individualised biomarker highlighted a combination of MD and A changes. For the MD, the sPCA formed a positive cluster around the Sylvian fissure on the left side from $z = -15$ to $z = +10$ in the MNI space including the temporal pole of the superior temporal gyrus (STG), portions of the opercular, triangular and orbital parts of the inferior frontal gyrus to finally reach the uncinate fasciculus. The A contributed to form some other negative clusters around the pons reaching the cerebellar peduncles fibers from the left side. The eigenvector of the decomposition in the sPCA space correlated negatively with a partial measure of alcohol consumption and with a measure of the histrionic part of personality disorder that were evaluated by the ASI and SCID scores as shown in Table 3, respectively.

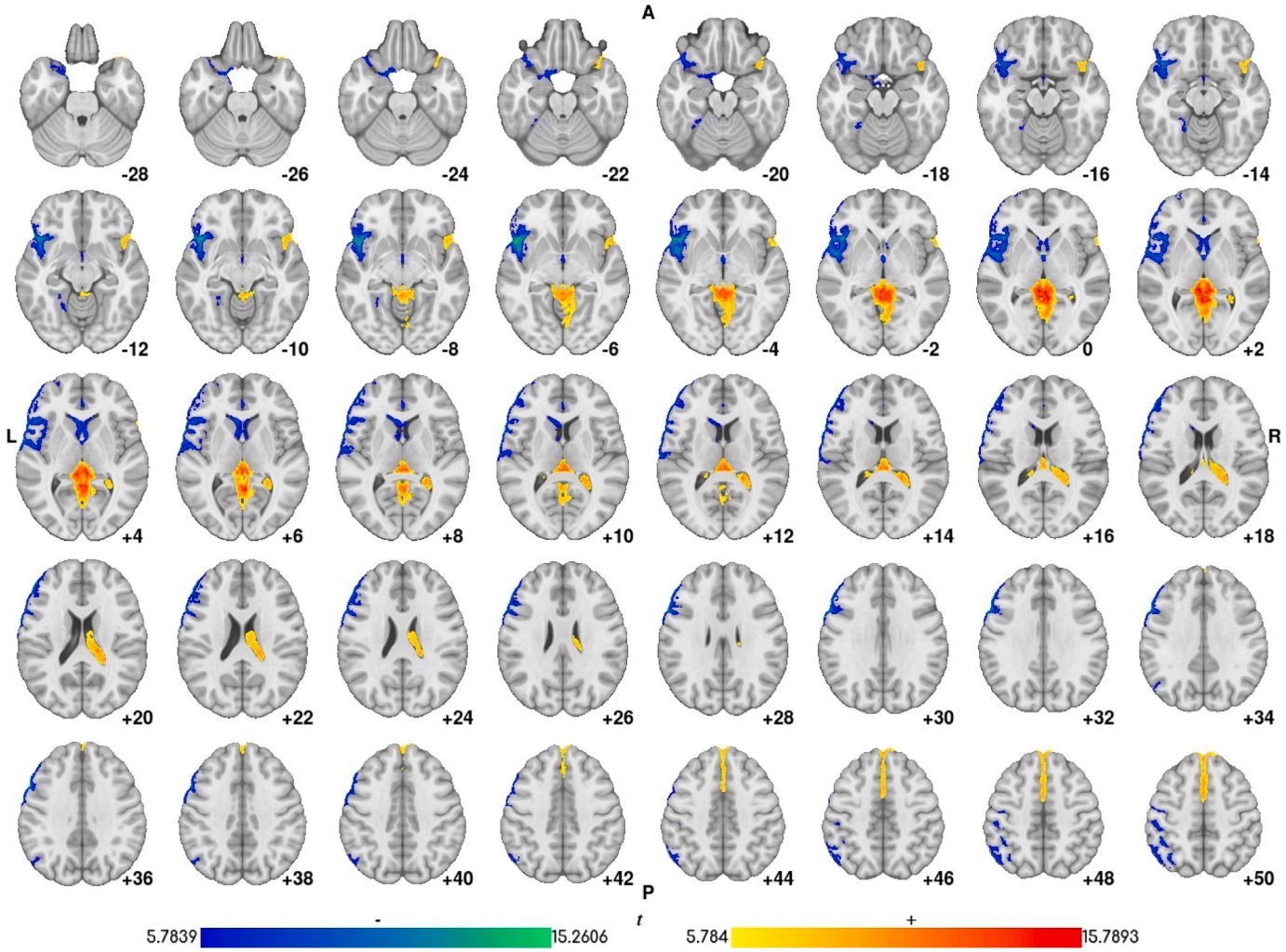

Fig. 3. Voxel-based diktiometry sensitivity results from $z = -28$ to $z = +50$ in MNI space for the fractional anisotropy (FA).

3.3.2. PC2

The second formed clusters relating to the combination of MD and PsPl. The voxels relative to the MD clustered mainly on the portion of the interhemispheric fissure proximal to the vermis, around the lingual gyrus reaching the calcarine fissure and reaching also the PCC-L, the PCC-R and a small portion of the sCC. The voxels relative to PsPl highlighted contributions around the ventral posterolateral (VPL) nuclei, the inferior pulvinar (PuI) and the medial geniculate nucleus (MGN) in the left thalamus. This component correlated negatively with the SCID-Schizoid personality disorder (Table 3).

3.3.3. PC3

The loadings of the third individualised biomarker formed positive clusters relative to A around the left hippocampus, the amygdala, the uncinate fasciculus and the inferior longitudinal fasciculus. Another positive cluster was found around the fusiform and the lingual gyrus of the left cerebellar hemisphere. The voxels clustered around portions of the vermis and the lobules IV, V and VI of the cerebellar hemisphere to form negative clusters relative to the A. The eigenvector of the third individualised biomarker correlated positively with the non-planning impulsiveness aspect of BIS as shown in Table 3.

3.3.4. PC4

The fourth individualised biomarker also clustered negative voxels relative to A starting around the MGN of the left thalamus and continued around the superior and inferior cerebellar peduncles fibers and the corticospinal tract from the left side to finally reach the vermis, the fusiform, the lingual gyrus and the cerebellar hemisphere (lobules III, IV, V and VI). The eigenvector of the decomposition correlated positively with the measures of the obsessive-compulsive and schizoid aspects of the SCID test; depression, interpersonal sensitivity, obsessive-compulsive and paranoid ideation that contributed to the global severity index aspects evaluated by the SCL-90; and the Get. Alone aspect from the WHODAS test shown in Table 3.

3.3.5. PC5

The fifth individualised biomarker was a combination of clusters relative to A and PsPl. For the sensitivity to A, sPCA formed clusters around the fibers of the superior cerebellar peduncles and the sCC, including portions of the PCC-L, hippocampus and the medial cingulate cortex passing through the cortico-ponto-cerebellar (CPC) pathway on the right. A second cluster was formed from portions of the ventral tegmental area (VTA) on both sides, the median and dorsal raphe nuclei (MRN, DRN), the vermis, and portions of lobules III, IV and V of the cerebellum. Similarly, the positive clusters relative to PsPl were located on portions of the sCC, bCC spanning through the PCC-L. We found a negative association of the fifth eigenvector and the attention aspect evaluated by the BIS questionnaire. The eigenvector was also found positively correlated with the avoidant, aspect of the SCID evaluation; and with anxiety, hostility, interpersonal sensitivity, obsessive-compulsive, paranoid ideation, phobic anxiety and psychoticism that contributed to the global severity index and the total of the positive

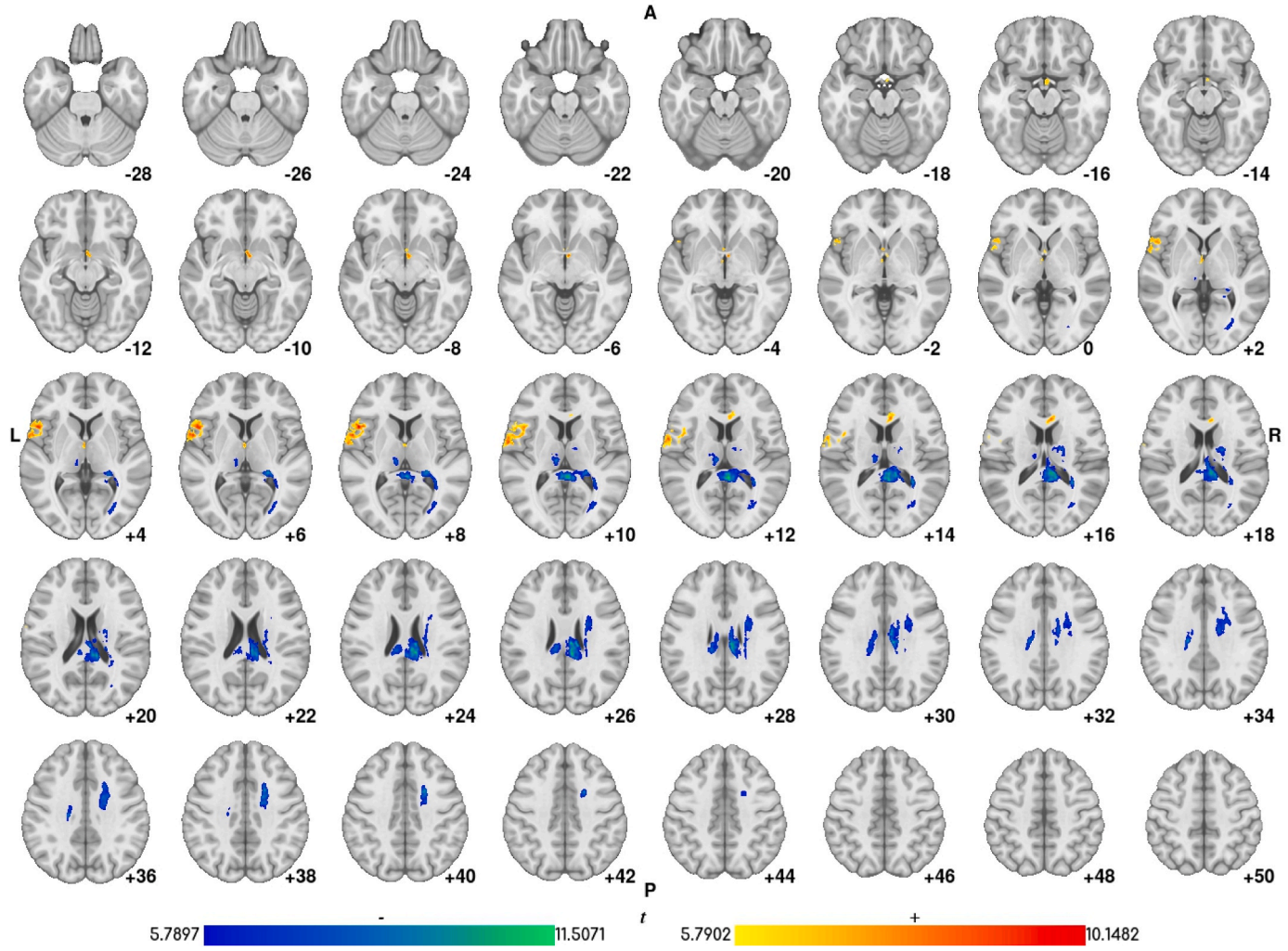

Fig. 4. Voxel-based diktiometry sensitivity results from $z = -28$ to $z = +50$ in MNI space for the anisotropy (A).

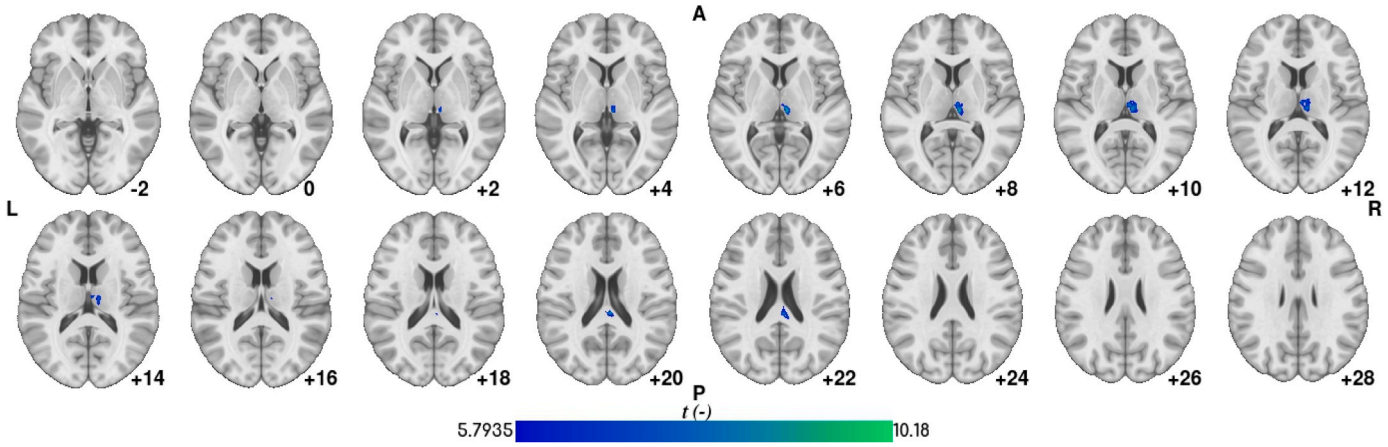

Fig. 5. Voxel-based diktiometry sensitivity results from $z = -2$ to $z = +28$ in MNI space for the pseudoplanarity (PsPl).

symptom evaluated by the SCL-90 questionnaire as shown in Table 3.

4. Discussion

VBD shows a lot of promise for the detection of non-linear and non-local biomarkers that are difficult to capture with traditional VBA. This is likely due to the large variability present in the CUD patient population in terms of addiction duration and severity, but also demographics and behaviour, which suggests that these patterns may be more or less present across patients.

sPCA has shown itself to be largely capable of disambiguating these results and highlighting the individual patterns that are the most highly

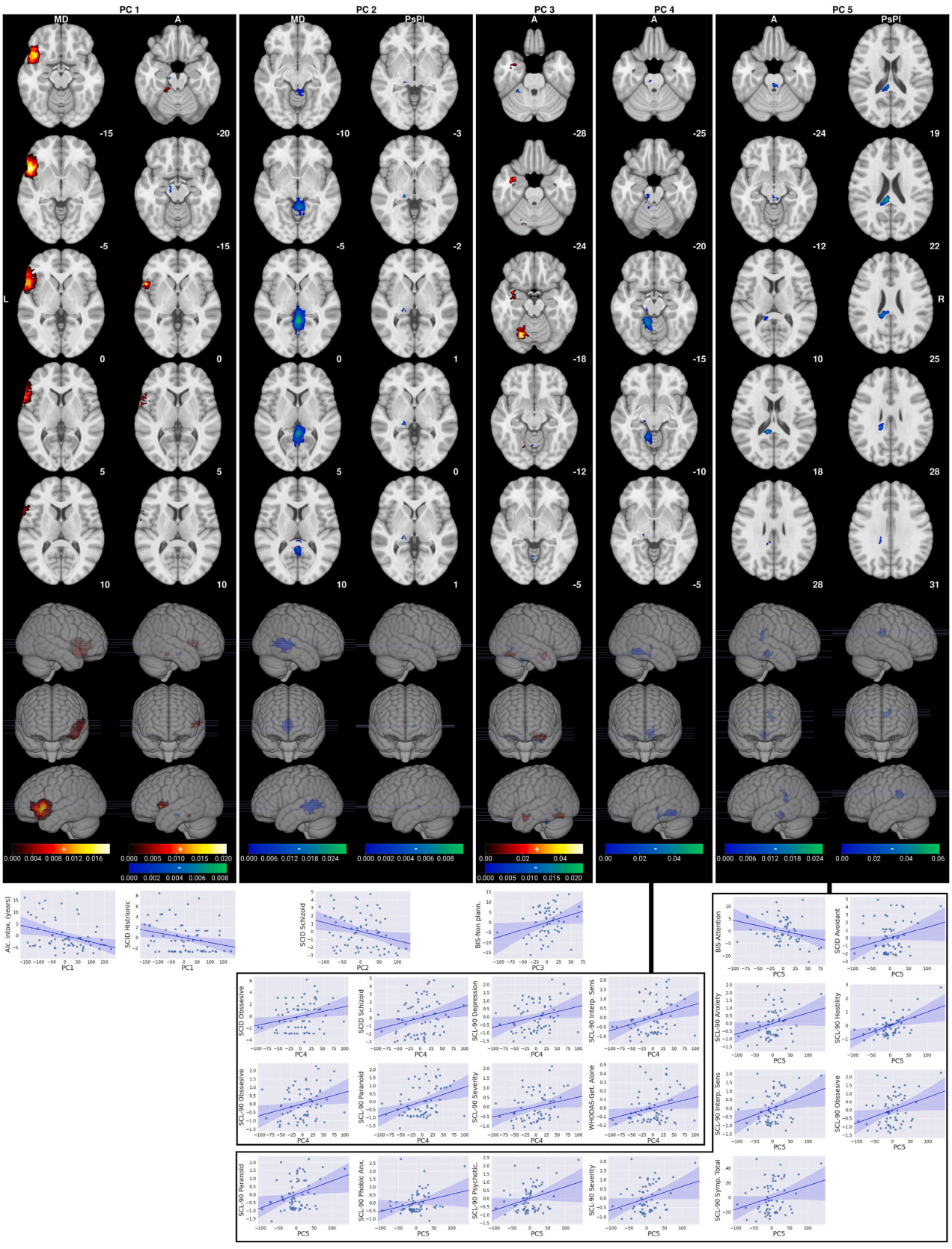

Fig. 6. Five principal components (PC) obtained by sparse principal components analysis on the sensitivity images relative to mean diffusivity (MD), anisotropy (A) and pseudo-planarity (PsPl). Each column shows the loading contribution to the diffusivity measure limited to clusters of size greater or equal to 128 mm^3. The fitting lines correlating the individual value along the principal component and the clinical scores using the age and sex as covariates ($p < 0.05$) are shown in the scatter plots.

Table 3
Partial correlation of the principal components (PC) from sparse principal components analysis with the clinical scores found significant at $p < 0.05$ after removing the effects of age and sex (r, p-value).

		PC1	PC2	PC3	PC4	PC5
Alcohol consumption ASI	Intox. (years)	(-0.34, 0.0069)				
Non-impulsive-impulsive behaviours BIS	Attention					(-0.2853, 0.0314)
	Non plann.			(0.2854, 0.0314)		
Personality disorders SCID-II for DSM-IV	Avoidant					(0.2426, 0.0479)
	Histrionic	(-0.2706, 0.0268)				
	Obsessive				(0.2451, 0.0456)	
	Schizoid		(-0.2879, 0.0181)		(0.2446, 0.0461)	
Psychological symptoms and distress SCL-90	Anxiety					(0.2629, 0.0374)
	Depression				(0.2621, 0.038)	
	Hostility					(0.499, 0.0)
	Interp. Sens				(0.2933, 0.0197)	(0.3266, 0.009)
	Obsessive				(0.2799, 0.0263)	(0.308, 0.0141)
	Paranoid				(0.357, 0.0041)	(0.3283, 0.0086)
	Phobic Anx.					(0.2818, 0.0253)
	Psychotic.					(0.3345, 0.0074)
	Severity				(0.2497, 0.0484)	(0.3012, 0.0164)
	Symp. Total					(0.2737, 0.03)
Disability assessment WHODAS	Get. Alone				(0.2533, 0.0386)	

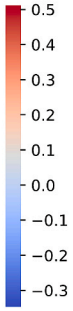

variable across patients. Our results showed that the majority of our CNN-derived imaging biomarkers can be decomposed into five separate biomarkers that are differentially expressed across the patient database. This strongly confirms our hypothesis that basic VBD does couple together distinctly different biomarkers for heterogeneous disorders, but that these biomarkers can be mathematically decoupled by looking at only correlated differences between the patients with the HC group removed.

4.1. *Diffusion characteristics and the effects of CUD*

The following sections discuss the VBD findings as well as their individualised biomarkers with respect to a particular neuroanatomical region. The goal is to use the various sensitivity maps in tandem to better interpret the precise mechanism observed by the CNN as well as its evidence in the literature. These regions largely involve the brain's decision-making brain circuitry, specifically the medial prefrontal cortex (mPFC), the posterior cingulate cortex (PCC), and ventral regions of the striatum (VS). However, this is not heterogeneous regardless of the nature of the reward. McClure et al. (2004) found that activation in the VS was specific to immediate, rather than delayed, rewards. Kable and Glimcher (2007) found that these regions were rather sensitive to the subjective value of the reward, conjecturing that immediate rewards could be seen as having a higher subjective value in the moment than delayed ones. These views were later reconciled by Sripada et al. (2011), although with some anatomical differences, showing that both immediacy and subjective value have distinct effects. Although this information has been collected using functional imaging (McClure et al., 2004; Kable and Glimcher, 2007; Sripada et al., 2011) and DTI does not capture said functional information, it does suggest some level of remodelling present in this region that distinguishes between CUD patients and HC.

4.1.1. *Insula and Sylvian fissure*

The region around the insula was identified as a positive cluster in both MD (Fig. 2) and A (Fig. 4) sensitivity maps. This indicates that there is an increased ratio of high MD and high A tissue in this region, specifically WM fibres. This is consistent with the literature on addiction that has found that addiction generally increases the WM-to-GM ratio in the insula (Naqvi and Bechara, 2009) and cortical thinning in the temporal lobe (Bittencourt et al., 2021) which can be detected on diffusion images. The increased salience of the MD correlation compared to that of A also likely indicates GM degeneration as that would additionally increase the local proportion of CSF (and that fissural expansion can be seen as indirect evidence of GM atrophy in the adjacent cortex), leading to an increased amount of nearly spherical diffusion.

Rather than general expansion, the expansion of the Sylvian fissure appears to be lateralised. This is evident in that the network assigns a negative sensitivity to the contralateral side which in VBD is a clear sign of an "asymmetry check" (Estudillo-Romero et al., 2022). The fact that the network uses an asymmetry check rather than only showing lateralised expansion is likely because the lateralised expansion is subtle and the size of the Sylvian fissure is highly variable across patients, thus using the opposite side as a reference is beneficial to this biomarker's detection. Asymmetry has recently been considered as being indicative of substance dependence, although at the moment it is not clear what direction this causal relation has, that is, whether substance addiction leads to this brain asymmetry or if this asymmetry facilitates addiction (W Gordon, 2016; Cao et al., 2021).

With respect to the individualised biomarkers, the insula is clearly the structure of interest for PC 1. From the correlation tests with clinical variables, there is a negative correlation between the relevance of this structure for identifying CUD and the patient's history of alcohol consumption. This is interesting as there is literature on the relationship between alcohol abuse and expansion of the Sylvian fissure (Le Berre et al., 2015) or GM thinning in adjacent structures (Pennington et al., 2015) which would have a similar diffusion pattern. What this suggests is that this particular biomarker becomes less useful to the CNNs as a distinct biomarker for CUD as alcohol dependence increases, which may be problematic as the two frequently co-occur (National Survey on Drug Use and Health, 2021). There is also some evidence that the presence of personality disorders from the cluster B, which includes antisocial, borderline, histrionic and narcissistic aspects, can change the connectivity besides to changes seen in CUD without these disorders

(Albein-Urios et al., 2013) which supports them being an individualised biomarker that varies across the patient population.

The insula has long been the target of neuroimaging investigations of substance use disorders including CUD. Moeller and Paulus (2018) found increased activity in the insula responding to rewards in people with CUD compared to controls which Paulus (2022) later suggests is robust across the substances being used. This supports our conclusion regarding PC 1 and alcohol use, specifically that these insular changes are reflective of general addiction (i.e. cocaine or alcohol use) rather than substance-specific. Although DTI is not sensitive to these functional signatures, our results as well as previous results in cortical thinning suggest that corresponding structural changes are indeed visible in DTI even if they are sub-voxel in scale.

4.1.2. Cerebellum

Given its low dopamine content, it has been common to exclude the cerebellum from the circuitry that mediates the stimulant-associated behaviours (Anderson et al., 2006), it has however been shown plasticity changes occurring in this structure after exposure and abstinence to cocaine (Vazquez-Sanroman et al., 2015) in animal models. Our results showing a cluster in the superior part of the left cerebellum suggest that cerebellar GM degeneration may be present. This observation is consistent with that made by Moreno-López et al. (2015) although somewhat less extensive than the results they found looking specifically at GM volume in T1-weighted structural MRI indicating that DTI is also sensitive to this degeneration.

In terms of individualised biomarkers, degeneration of the cerebellum appears to be orthogonal from the other biomarkers as it is concentrated in PC 3 and PC 4, indicating that it is not a singular biomarker but rather two orthogonal ones with significant patient variability. PC 3 is associated with impulsivity and PC 4 is associated with a variety of personality and psychological symptoms. Experiments on healthy subjects have provided evidence of the existence of a cortico-limbic-cerebellar circuit participating in cognitive/emotional tasks (Belkhiria et al., 2017) associated with aggression (Wolfs et al., 2022). This could partially explain these results as well as the attentional impulsivity and hostility correlate within the cerebellar clusters obtained from PC5 on CUD patients.

4.1.3. WM tracts and the ventricles

One of the most notable limitations of the use of VBD more generally is it does not test a particular hypothesis (e.g. that a change in a particular characteristic in a particular region is correlated with a particular disorder) which implies that the computer is more likely to find larger scale changes that are more easily extracted from the data, rather than subtler ones. In the case of CUD, it appears that the CNNs principally observed features of the ventricular and CSF systems (i.e. their expansion), rather than using diffusion information to make inferences about white mater bundles.

There is some evidence that patient-specific ventricular size (which is observed in the MD images consistently across all patients in Fig. 2, slices −14 to +28) correlates with the individual's response to cocaine (Bartzokis et al., 2000). This complicates the narrative as this particular patient property could lead to, rather than result from, differences in cocaine use leading to its heightened expression in CUD patients.

Some information can be seen that specifically relates to WM alterations in the A sensitivity maps, specifically in the posterior region of the corpus callosum (Fig. 4 slices +8 to +28) and a thin elongated region, likely one or more WM bundles, on the right side extending superiorly from the lateral thalamus to the posterior frontal lobe (Fig. 4 slices +10 to +28). As this particular approach is not tractographic, it is unclear as to where these bundles terminate as it is possible that only a portion of the bundles has been identified. One possibility is that it is the frontal portions of the thalamocortical radiations which are known to be affected by addiction, specifically to methamphetamines (Uhlmann et al., 2016) and video games (Jeong et al., 2016). The precise mechanisms through which cocaine affects the brain, including the corpus callosum, are complex and multifaceted. The use of cocaine can lead to changes in neurotransmitter systems, neuroinflammation, and alterations in neuroplasticity, all of which can contribute to the observed brain changes (Hodges et al., 2023).

The corpus callosum is also important in the individualised biomarker PC 5, specifically in terms of microstructural alteration (as shown through A and PsPl rather than MD) which is associated with almost all the psychological symptoms measured in the cohort. This is consistent with observations in the literature connecting these psychological symptoms and changes in the corpus callosum (Jiang et al., 2017; Sadek et al., 2021; Zhang et al., 2017) and disorders reflecting these symptoms may increase the likelihood of CUD rather than result from it. There are also numerous papers directly investigating the corpus callosum solely in terms of CUD (Hodges et al., 2023) although these may also be subject to the same limitations in terms of confounding findings in personality disorders.

4.1.4. Subcortical gray matter

Interestingly, the medial nuclei of the right thalamus has also been marked as significant due to changes in PsPl which measures how planar the diffusion tensor can be, constrained by having a particular MD and A. This indicates a degree of complex micro-structural change that would need to be further investigated, especially due to the wide connectivity of the region with areas of the anterior cingulate cortex and nucleus accumbens already known to be implicated in CUD as part of the reward circuitry (Cooper et al., 2017). One hypothesis is that this is caused by differences in the proportion of connections with respect to different regions which result in an overall change in the coarse-grained shape of the tensor (averaging together the diffusion of several tracks extending in different directions). This may explain why the pseudo-planarity is affected more so than other diffusion characteristics.

4.2. Limitations

4.2.1. Complexity of the patient distribution

One of the fundamental issues with analysing a disorder such as CUD is its complex relationship to numerous socio-economic factors which could confound a simple interpretation of any analysis (Malinowska and Żuradzki, 2022). Although this dataset was collected with a view towards controlling for some of these variables, notably gender and addiction to other substances (See Table 1), other important demographic and socio-economic variables regarding racialisation were not included, which are likely important to ensuring representative distributions for CUD (Malinowska and Żuradzki, 2022).

4.2.2. Model complexity and performance

The primary technical limitation of this work is the reliance on an ensemble of traditional, relatively simple CNNs. Although easier to analyse, this network has a lower classification performance than more recent neural network models for image classification. One of the reasons for preferring such a framework is the limited amount of training data available which would be problematic if used to train models with heavier parameterisation. The collection of more data would not only improve the capabilities of our existing framework but also allow us to augment it with more performant CNNs.

The model performance is coherent with the general literature on detecting CUD from imaging modalities alone (Li et al., 2020) as well as using DTI alone to detect neurological disorders such as Alzheimer's disease (Ebadi et al., 2017), major depression (Yang et al., 2022), and Parkinson's disease (Sharma et al., 2020; Estudillo-Romero et al., 2022), all of which display accuracies on the order of 60%–80%. This suggests that DTI as a modality and the heterogeneity of CUD patients may be limiting features as multimodal machine learning studies on other neurological disease patient populations have received higher classification accuracies (Lima et al., 2022).

In terms of decomposing the VBD results into individualised biomarkers, sPCA is a well-known and robust machine learning technique. Thus, its efficacy indicates that simpler linear machine learning methods remain highly important for the use of artificial intelligence in neuroimaging.

4.2.3. Interpretation complexity

As noted in Section 3.2, the CNN model is flexible enough to find many different features visible in DTI that are not strictly related to microstructural diffusion. For example, we interpreted the positive sensitivity seen in the lateral ventricles as the expansion of a high-diffusion region of CSF rather than as a change in the diffusivity of CSF itself. Similarly, because the biomarkers are non-local, they could reflect multiple regions, preventing them from being judged individually. For example, we argued that there likely isn't a contraction of the right Sylvian fissure but rather that the network is looking for an asymmetry in Sylvian fissure expansion which is more severe on the left side. This additional reasoning comes from basic neuroanatomical knowledge as well as an appreciation for the literature in this domain rather than from the CNN model itself. This task of interpretation is a particular limitation of the type of black-box reasoning performed by modern deep learning techniques. Although we have attempted to alleviate this problem, notably through an approach to decoupling features that differ across patients using sPCA, these automated approaches are not perfect and still leave a large amount of the task of interpretation to human experts.

4.3. Future work

One current concern regarding VBD biomarkers and their individualised versions is that they only indicate the degree to which these artificial neural networks are sensitive to particular characteristics of particular brain regions. This means that they indicate the existence and relevance of a biomarker but not its expression. This is particularly important when considering individualised biomarkers as what is being measured is not the different expression of a biomarker but its differential relevance. An important area of future work is to develop methods that also measure the patient's expression of a particular biomarker, which would significantly assist in distinguishing between the multiple potential causes of this differential relevance.

Lastly, due to the preliminary nature of the study, the complexity of machine learning methods and the ambiguity in the interpretation of the features, it is necessary to re-validate the approach on an independent dataset such as those from the Human Connectome Project (Elam et al., 2021) or the ENIGMA Working Group (Chye et al., 2020), both of which include information on substance use disorders. This re-validation should include accuracy measurements from the CNN ensemble, showing that it is truly detecting CUD and not some a spurious correlation specific to the SUDMEX CONN database used as training data. Another related area of technical research would be the use of techniques such as model distillation (Gou et al., 2021) to create simpler and more clinically useful algorithms that instantiate the biomarkers discovered through VBD. This would significantly facilitate the reproducibility of complex non-local methods by allowing them to be more readily applied on new, independent data. Thus, re-validation involves not only the acquisition of more multi-centric data, but also new technical development.

5. Conclusions

Voxel-based diktiometry is an emerging technique for using advanced machine learning algorithms to automatically detect complex and non-local imaging biomarkers for neurological disorders. This technique is completely unguided, allowing for the computer to detect whatever biomarkers that it finds to be the most salient for distinguishing between patients with CUD and HC. In the past, the principal problem with this technique arose from said unguided complexity and non-locality: it is possible for distinctly different biomarkers to be merged together, masking the heterogeneity of the disorder under investigation and making the interpretation of these biomarkers more difficult.

Not only is this the first article to propose machine-learning derived DTI biomarkers for CUD, it also alleviates part of the aforementioned difficulty, showing how the individual sensitivity maps that feed into VBD analysis can be decomposed along a series of automatically learnt regions that express the extent of patient variability as well as where said variability arises from. For CUD, our analysis shows that we have a highly variable patient population who expresses at least five well-separated addiction biomarkers. These individualised biomarkers target particular coherent regions of the brain and are also associated with various psychological and personality tests that may correlate with different levels of addiction.

These tools offer a new approach to discovering biomarkers explaining the effect of CUD on the brain in a way that is entirely guided by the data itself.

CRediT authorship contribution statement

Alfonso Estudillo-Romero: Writing – original draft, Visualization, Validation, Software, Methodology, Data curation. **Raffaella Migliaccio:** Writing – review & editing, Writing – original draft, Validation. **Bénédicte Batrancourt:** Writing – review & editing, Writing – original draft, Validation, Conceptualization. **Pierre Jannin:** Writing – review & editing, Supervision. **John S.H. Baxter:** Writing – review & editing, Writing – original draft, Supervision, Methodology.

Declaration of competing interest

The authors declare that they have no known competing financial interests or personal relationships that could have appeared to influence the work reported in this paper.

Data availability

Data was from an open online repository (SUDMEX CONN)

Acknowledgements

Alfonso Estudillo Romero is supported through the Fondation Recherche Médicale (FRM) DIC20161236441, the SAD Région Bretagne programme, and the Institut des Neurosciences Cliniques de Rennes (INCR).

References

Albein-Urios, N., Verdejo-Román, J., Soriano-Mas, C., Asensio, S., Martínez-González, J. M., Verdejo-García, A., 2013. Cocaine users with comorbid cluster b personality disorders show dysfunctional brain activation and connectivity in the emotional regulation networks during negative emotion maintenance and reappraisal. Eur. Neuropsychopharmacol 23, 1698–1707.

Anderson, C.M., Maas, L.C., Frederick, B.d., Bendor, J.T., Spencer, T.J., Livni, E., Lukas, S.E., Fischman, A.J., Madras, B.K., Renshaw, P.F., Kaufman, M.J., 2006. Cerebellar vermis involvement in cocaine-related behaviors. Neuropsychopharmacology 31, 1318–1326.

Andersson, J.L.R., Sotiropoulos, S.N., 2016. An integrated approach to correction for off-resonance effects and subject movement in diffusion MR imaging. Neuroimage 125, 1063–1078.

Angeles-Valdez, D., Rasgado-Toledo, J., Issa-Garcia, V., Balducci, T., Villicaña, V., Valencia, A., Gonzalez-Olvera, J.J., Reyes-Zamorano, E., Garza-Villarreal, E.A., 2022. The Mexican magnetic resonance imaging dataset of patients with cocaine use disorder: SUDMEX CONN. Sci. Data 9, 133.

Avants, B., Epstein, C., Grossman, M., Gee, J., 2008. Symmetric diffeomorphic image registration with cross-correlation: evaluating automated labeling of elderly and neurodegenerative brain. Med. Image Anal. 12, 26–41.

Avants, B.B., Tustison, N.J., Song, G., Cook, P.A., Klein, A., Gee, J.C., 2011. A reproducible evaluation of ANTs similarity metric performance in brain image registration. Neuroimage 54, 2033–2044.

Bartzokis, G., Beckson, M., Lu, P.H., Edwards, N., Rapoport, R., Wiseman, E., Bridge, P., 2000. Increased csf volumes are associated with diminished subjective responses to cocaine infusion. Neuropsychopharmacology 23, 468–473.
Belkhiria, C., Driss, T., Habas, C., Jaafar, H., Guillevin, R., De Marco, G., 2017. Exploration and identification of cortico-cerebellar-brainstem closed loop during a motivational-motor task: an fMRI study. Cerebellum 16, 326–339.
Bittencourt, A.M.L., Bampi, V.F., Sommer, R.C., Schaker, V., Juruena, M.F.P., Soder, R.B., Franco, A.R., Sanvicente-Vieira, B., Grassi-Oliveira, R., Ferreira, P.E.M.S., 2021. Cortical thickness and subcortical volume abnormalities in male crack-cocaine users. Psychiatr. Res. Neuroimaging 310, 111232.
Cao, Z., Ottino-Gonzalez, J., Cupertino, R.B., Schwab, N., Hoke, C., Catherine, O., Cousijn, J., Dagher, A., Foxe, J.J., Goudriaan, A.E., et al., 2021. Mapping cortical and subcortical asymmetries in substance dependence: findings from the enigma addiction working group. Addiction Biol. 26, e13010.
Ceceli, A.O., Bradberry, C.W., Goldstein, R.Z., 2022. The neurobiology of drug addiction: cross-species insights into the dysfunction and recovery of the prefrontal cortex. Neuropsychopharmacology 47, 276–291.
Chye, Y., Mackey, S., Gutman, B.A., Ching, C.R., Batalla, A., Blaine, S., Brooks, S., Caparelli, E.C., Cousijn, J., Dagher, A., et al., 2020. Subcortical surface morphometry in substance dependence: an enigma addiction working group study. Addiction Biol. 25, e12830.
Cooper, S., Robison, A., Mazei-Robison, M.S., 2017. Reward circuitry in addiction. Neurotherapeutics 14, 687–697.
Ebadi, A., Dalboni da Rocha, J.L., Nagaraju, D.B., Tovar-Moll, F., Bramati, I., Coutinho, G., Sitaram, R., Rashidi, P., 2017. Ensemble classification of alzheimer's disease and mild cognitive impairment based on complex graph measures from diffusion tensor images. Front. Neurosci. 11, 56.
Elam, J.S., Glasser, M.F., Harms, M.P., Sotiropoulos, S.N., Andersson, J.L., Burgess, G.C., Curtiss, S.W., Oostenveld, R., Larson-Prior, L.J., Schoffelen, J.M., et al., 2021. The human connectome project: a retrospective. Neuroimage 244, 118543.
Estudillo-Romero, A., Haegelen, C., Jannin, P., Baxter, J.S.H., 2022. Voxel-based diktiometry: combining convolutional neural networks with voxel-based analysis and its application in diffusion tensor imaging for Parkinson's disease. Hum. Brain Mapp. 1–17.
Gaudreault, P.O., King, S.G., Malaker, P., Alia-Klein, N., Goldstein, R.Z., 2023. Whole-brain white matter abnormalities in human cocaine and heroin use disorders: association with craving, recency, and cumulative use. Mol. Psychiatr. 28, 780–791.
Gou, J., Yu, B., Maybank, S.J., Tao, D., 2021. Knowledge distillation: a survey. Int. J. Comput. Vis. 129, 1789–1819.
Hammond, C.J., Allick, A., Rahman, N., Nanavati, J., 2019. Structural and functional neural targets of addiction treatment in adolescents and young adults: a systematic review and meta-analysis. J. Child Adolesc. Psychopharmacol. 29, 498–507.
Hodges, C.B., Steinberg, J.L., Zuniga, E.A., Ma, L., Bjork, J.M., Moeller, F.G., 2023. Chronic cocaine use and white matter coherence: a diffusion tensor imaging study. J. Stud. Alcohol Drugs jsad–21.
Hulka, L.M., Vonmoos, M., Preller, K.H., Baumgartner, M.R., Seifritz, E., Gamma, A., Quednow, B.B., 2015. Changes in cocaine consumption are associated with fluctuations in self-reported impulsivity and gambling decision-making. Psychol. Med. 45, 3097–3110.
Jeong, B.S., Han, D.H., Kim, S.M., Lee, S.W., Renshaw, P.F., 2016. White matter connectivity and internet gaming disorder. Addiction Biol. 21, 732–742.
Jiang, W., Shi, F., Liu, H., Li, G., Ding, Z., Shen, H., Shen, C., Lee, S.W., Hu, D., Wang, W., et al., 2017. Reduced white matter integrity in antisocial personality disorder: a diffusion tensor imaging study. Sci. Rep. 7, 43002.
Jiménez, S., Angeles-Valdez, D., Villicaña, V., Reyes-Zamorano, E., Alcala-Lozano, R., Gonzalez-Olvera, J.J., Garza-Villarreal, E.A., 2019. Identifying cognitive deficits in cocaine dependence using standard tests and machine learning. Prog. Neuro Psychopharmacol. Biol. Psychiatr. 95, 109709.
Kable, J.W., Glimcher, P.W., 2007. The neural correlates of subjective value during intertemporal choice. Nat. Neurosci. 10, 1625–1633.
Koob, G.F., Volkow, N.D., 2010. Neurocircuitry of addiction. Neuropsychopharmacology 35, 217–238.
Le Berre, A.P., Pitel, A.L., Chanraud, S., Beaunieux, H., Eustache, F., Martinot, J.L., Reynaud, M., Martelli, C., Rohlfing, T., Pfefferbaum, A., et al., 2015. Sensitive biomarkers of alcoholism's effect on brain macrostructure: similarities and differences between France and the United States. Front. Hum. Neurosci. 9, 354.
Lesage, E., Stein, E.A., 2016. Networks associated with reward. In: Pfaff, D.W., Volkow, N.D. (Eds.), Neuroscience in the 21st Century. Springer, New York, New York, NY, pp. 1–27.
Li, D., Yang, B., Gu, X., Kong, D., Zan, P., 2020. Drug addiction detection algorithm based on cnn-bn. In: Proceedings of the 2020 9th International Conference on Computing and Pattern Recognition, pp. 96–100.
Lima, A.A., Mridha, M.F., Das, S.C., Kabir, M.M., Islam, M.R., Watanobe, Y., 2022. A comprehensive survey on the detection, classification, and challenges of neurological disorders. Biology 11, 469.
Mairal, J., Bach, F., Ponce, J., Sapiro, G., 2009. Online dictionary learning for sparse coding. In: Proceedings of the 26th Annual International Conference on Machine Learning. ACM, Montreal Quebec Canada, pp. 689–696.
Malinowska, J.K., Żuradzki, T., 2022. Towards the multileveled and processual conceptualisation of racialised individuals in biomedical research. Synthese 201, 11.
McClure, S.M., Laibson, D.I., Loewenstein, G., Cohen, J.D., 2004. Separate neural systems value immediate and delayed monetary rewards. Science 306, 503–507. https://doi.org/10.1126/science.1100907.
McHugh, M.J., Demers, C.H., Braud, J., Briggs, R., Adinoff, B., Stein, E.A., 2013. Striatal-insula circuits in cocaine addiction: implications for impulsivity and relapse risk. Am. J. Drug Alcohol Abuse 39, 424–432.
Mclellan, A.T., Kushner, H., Metzger, D., Peters, R., Pettinati, H., Argeriou, M., 1992. The fifth edition of the addiction severity index. J. Subst. Abuse Treat. 9, 199–213.
Moeller, S.J., Paulus, M.P., 2018. Toward biomarkers of the addicted human brain: using neuroimaging to predict relapse and sustained abstinence in substance use disorder. Prog. Neuro Psychopharmacol. Biol. Psychiatr. 80, 143–154.
Moreno-López, L., Perales, J.C., van Son, D., Albein-Urios, N., Soriano-Mas, C., Martinez-Gonzalez, J.M., Wiers, R.W., Verdejo-García, A., 2015. Cocaine use severity and cerebellar gray matter are associated with reversal learning deficits in cocaine-dependent individuals. Addiction Biol. 20, 546–556.
Naqvi, N.H., Bechara, A., 2009. The hidden island of addiction: the insula. Trends Neurosci. 32, 56–67.
National Survey on Drug Use and Health, 2021. Key Substance Use and Mental Health Indicators in the United States: Results from the 2021 National Survey on Drug Use and Health.
Norton, I., Essayed, W.I., Zhang, F., Pujol, S., Yarmarkovich, A., Golby, A.J., Kindlmann, G., Wassermann, D., Estepar, R.S.J., Rathi, Y., Pieper, S., Kikinis, R., Johnson, H.J., Westin, C.F., O'Donnell, L.J., 2017. SlicerDMRI: open source diffusion MRI software for brain cancer research. Cancer Res. 77, e101–e103.
Paulus, M.P., 2022. Neural substrates of substance use disorders. Curr. Opin. Neurol. 35, 460–466.
Peacock, A., Leung, J., Larney, S., Colledge, S., Hickman, M., Rehm, J., Giovino, G.A., West, R., Hall, W., Griffiths, P., et al., 2018. Global statistics on alcohol, tobacco and illicit drug use: 2017 status report. Addiction 113, 1905–1926.
Pennington, D.L., Durazzo, T.C., Schmidt, T.P., Abé, C., Mon, A., Meyerhoff, D.J., 2015. Alcohol use disorder with and without stimulant use: brain morphometry and its associations with cigarette smoking, cognition, and inhibitory control. PLoS One 10, e0122505.
Pujol, S., Wells, W., Pierpaoli, C., Brun, C., Gee, J., Cheng, G., Vemuri, B., Commowick, O., Prima, S., Stamm, A., Goubran, M., Khan, A., Peters, T., Neher, P., Maier-Hein, K.H., Shi, Y., Tristan-Vega, A., Veni, G., Whitaker, R., Styner, M., Westin, C.F., Gouttard, S., Norton, I., Chauvin, L., Mamata, H., Gerig, G., Nabavi, A., Golby, A., Kikinis, R., 2015. The DTI challenge: toward standardized evaluation of diffusion tensor imaging tractography for neurosurgery: the DTI challenge on tractography for neurosurgery. J. Neuroimaging 25, 875–882.
Rasgado-Toledo, J., Shah, A., Ingalhalikar, M., Garza-Villarreal, E.A., 2022. Neurite orientation dispersion and density imaging in cocaine use disorder. Prog. Neuro Psychopharmacol. Biol. Psychiatr. 113, 110474.
Sadek, M.N., Ismail, E.S., Kamel, A.I., Saleh, A.A., Youssef, A.A., Madbouly, N.M., 2021. Diffusion tensor imaging of corpus callosum in adolescent females with borderline personality disorder. J. Psychiatr. Res. 138, 272–279.
Sharma, H., Soltaninejad, S., Cheng, I., 2020. Automated classification of Parkinson's disease using diffusion tensor imaging data. In: Advances in Visual Computing: 15th International Symposium, ISVC 2020, San Diego, CA, USA, October 5–7, 2020, Proceedings, Part II 15. Springer, pp. 658–669.
Spronk, D.B., van Wel, J.H., Ramaekers, J.G., Verkes, R.J., 2013. Characterizing the cognitive effects of cocaine: a comprehensive review. Neurosci. Biobehav. Rev. 37, 1838–1859.
Sripada, C.S., Gonzalez, R., Luan Phan, K., Liberzon, I., 2011. The neural correlates of intertemporal decision-making: contributions of subjective value, stimulus type, and trait impulsivity: neural Correlates of Intertemporal Decision-Making. Hum. Brain Mapp. 32, 1637–1648.
Suchting, R., Beard, C.L., Schmitz, J.M., Soder, H.E., Yoon, J.H., Hasan, K.M., Narayana, P.A., Lane, S.D., 2021. A meta-analysis of tract-based spatial statistics studies examining white matter integrity in cocaine use disorder. Addiction Biol. 26, e12902.
Tondo, L.P., Viola, T.W., Fries, G.R., Kluwe-Schiavon, B., Rothmann, L.M., Cupertino, R., Ferreira, P., Franco, A.R., Lane, S.D., Stertz, L., Zhao, Z., Hu, R., Meyer, T., Schmitz, J.M., Walss-Bass, C., Grassi-Oliveira, R., 2021. White matter deficits in cocaine use disorder: convergent evidence from in vivo diffusion tensor imaging and ex vivo proteomic analysis. Transl. Psychiatry 11, 1–13.
Uhlmann, A., Fouche, J.P., Lederer, K., Meintjes, E.M., Wilson, D., Stein, D.J., 2016. White matter microstructure and impulsivity in methamphetamine dependence with and without a history of psychosis. Hum. Brain Mapp. 37, 2055–2067.
Vazquez-Sanroman, D., Leto, K., Cerezo-Garcia, M., Carbo-Gas, M., Sanchis-Segura, C., Carulli, D., Rossi, F., Miquel, M., 2015. The cerebellum on cocaine: plasticity and metaplasticity. Addiction Biol. 20, 941–955.
W Gordon, H., 2016. Laterality of brain activation for risk factors of addiction. Curr. Drug Abuse Rev. 9, 1–18.
Wei, L., Wu, G.R., Bi, M., Baeken, C., 2021. Effective connectivity predicts cognitive empathy in cocaine addiction: a spectral dynamic causal modeling study. Brain Imag. Behav. 15, 1553–1561.
Wolfs, E.M.L., Klaus, J., Schutter, D.J.L.G., 2022. Cerebellar grey matter volumes in reactive aggression and impulsivity in healthy volunteers. Cerebellum 22, 223–233.
Yang, Y., Yang, Y., Pan, A., Xu, Z., Wang, L., Zhang, Y., Nie, K., Huang, B., 2022. Identifying depression in Parkinson's disease by using combined diffusion tensor imaging and support vector machine. Front. Neurol. 13, 878691.
Zhang, T., Wang, D., Zhang, Q., Wu, J., Lv, J., Shi, L., 2017. Supervoxel-based statistical analysis of diffusion tensor imaging in schizotypal personality disorder. Neuroimage 163, 368–378.
Zhao, Y., Sallie, S.N., Cui, H., Zeng, N., Du, J., Yuan, T., Li, D., De Ridder, D., Zhang, C., 2021. Anterior cingulate cortex in addiction: new insights for neuromodulation. Neuromodulation: Tech. Neural Interf. 24, 187–196.
Zou, H., Hastie, T., Tibshirani, R., 2006. Sparse principal component analysis. J. Comput. Graph Stat. 15, 265–286.